Monte Carlo methods used in inverted hexagonal lipid phase and in simulations of thermally fluctuating lipid vesicles

Samo Penič, Šárka Perutková, Miha Fošnarič & Aleš Iglič

International Journal of Advances in Engineering Sciences and Applied Mathematics

ISSN 0975-0770

Int J Adv Eng Sci Appl Math
DOI 10.1007/s12572-016-0164-3

Springer

Int J Adv Eng Sci Appl Math
DOI 10.1007/s12572-016-0164-3

Monte Carlo methods used in inverted hexagonal lipid phase and in simulations of thermally fluctuating lipid vesicles

Samo Penič[1] · Šárka Perutková[1] · Miha Fošnarič[1] · Aleš Iglič[1]

Abstract Two different uses of Monte Carlo methods in soft matter physics are presented in the following work. Firstly, the Monte Carlo simulated annealing is used to minimize the elastistic energy of the inverted hexagonal phase (H_{II}) optimal geometry. We will do a brief overview on the mechanics of the H_{II} lipid phase. In our model the expression for the lipid monolayer free energy consists of two energy contributions: the bending energy which involves also a deviatoric term, and the interstitial energy which describes the deformation energy due to stretching of the phospholipid molecule chains. On the basis of the derived expression for the lipid monolayer free energy, we will theoretically predict optimal geometry and physical conditions for the stability of the inverted hexagonal phase. Using the Monte Carlo simulated annealing method, we will theoretically describe first steps in the $L\alpha H_{II}$ phase transition. Another interesting subject investigated by means of Monte Carlo simulations are the thermal fluctuations of nearly spherical vesicles. The theoretical basis of this analysis was done by Milner and Safran (Phys Rev A 36(9):4371–4379, 1987. doi:10.1103/PhysRevA.36.4371) that uses the mean field approximation. In this work we will show the application of the Monte Carlo simulations and show the correlation between the time mean simulated thermal fluctuations decomposed into spherical harmonics and the bending stiffness in 2-dimensional and 3-dimensional space.

✉ Samo Penič
samo.penic@fe.uni-lj.si

Aleš Iglič
ales.iglic@fe.uni-lj.si

[1] Faculty of Electrical Engineering, University of Ljubljana, Tržaška 25, 1000 Ljubljana, Slovenia

Keywords Monte Carlo methods · Simulations · Phospholipid membrane · Inverted hexagonal phase · Bending stiffness

1 Introduction

Biological cells are enveloped by thin membrane, so-called plasma membrane [1]. The plasma membrane is enclosing the cell and shielding it from the extracellular surrounding already since the first prokaryotes developed [2]. It consists of lipid, protein and sugar molecules. A soft and fluid backbone of plasma membrane is the lipid bilayer in which proteins and sugars are embedded, and are in general free to move in lateral direction and also jump between both lipid layers (flip-flops). The cell membrane has crucial functions for cell life, i.e. it acts as a semipermeable barrier which controls the supply of the cell with different molecules through active or passive transport [2]. The membrane enables cell communication through glycolipid molecules on its surface. In eucaryotic cells the membrane also encloses organelles in cytoplasm. Furthermore, on membrane surface, the synthesis of ATP is taking place. The membrane electrical properties are also important for cell functioning and play and important role in fission and fusion of cells.

Lipid bilayer is a self-assembled structure of amphiphilic lipids. The most abundant sort of membrane lipids are phosphoglycerides. They consist of glycerol backbone where phosphate group is attached to the 3rd carbon through ester bond and first and second carbon ends are esterified by two long chain fatty acids. On its other end, the phosphate group is esterified by alcohol or amino alcohol, such as choline, ethanolamine, serine, inositol or glycerol, see Fig. 1 [3]. Another frequent membrane

Published online: 24 February 2016

phospholipids are sphingomyelines which have sphingosine as the backbone instead of glycerol.

The characteristic structure of lipid bilayer is stable due to hydrophobic effect. Amphiphatic membrane lipid molecule consists of two different moieties: polar lipid head group which is hydrophilic, can create hydrogen bonds with neighboring water molecules [1]. On the other hand, fatty acid chains are hydrophobic and cannot make bonds with the water molecules. Thus when pure phospholipid molecules are spreaded in water they self-assemble into clusters. In order to lower their free energy they hide hydrophobic chains from water and self-assemble into different structures. According to different conditions such as concentration, temperature or pH they self-assemble into micelles, lipid bilayers which closed themselves into spherical vesicles or other more complicated three dimensional structures such as cubic or hexagonal mesophases [4].

The unique and very important characteristic of membrane lipids is that unlike proteins, sugars, nuclear acids, where their building blocks are linked by chemical bonds (usually covalent), membrane lipids spontaneously create assemblies that are held together by much weaker interactions—the hydrophobic interactions, screened electrostatic forces, hydrogen bonds and van der Waals forces.

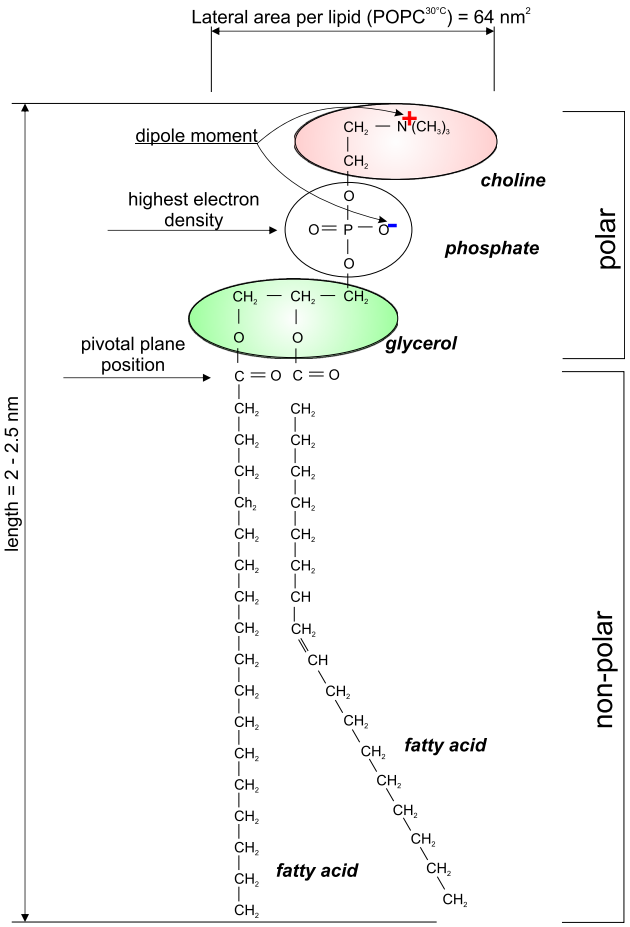

Fig. 1 Phospholipid molecule of POPC is shown schematically. Some physically relevant data are shown on the *left*

From the point of view of physicists, a biological membrane or even a simple lipid bilayer is therefore very interesting structure. It is a semipermeable barrier with structural and functional asymmetry. Lipid bilayers have very specific electrical properties such as conductivity and capacitance. The self-assembling properties lipid bilayers may be treated as liquid crystals of smectic type [5]. Therefore many physical properties can be theoretically described within different soft matter physics theories. In fact, the first liquid crystalline phase ever recorded were regularly stacked layers of myelin membranes. Myelin is a biological material that coats nerve fibers [6].

Computational algorithms often used in soft matter physics are Monte Carlo methods. They are used, for example, as optimization methods in multi-parameter phase-space, or for generating draws from appropriate probability distributions. In this work we present an example of each of the above mentioned uses of Monte Carlo simulations, applied on two quite distinct phospholipid structures.

First, in Sect. 2, we present the analysis of an inverted hexagonal phase as an example of non-lamellar phospholipid self-assembly structures, where we used simulated annealing Monte Carlo optimization method [7].

Then, in Sect. 3, we present Monte Carlo simulations of thermal fluctuations of phospholipid vesicle and its analysis for obtaining membrane elastic properties as previously reported in [8, 9]. Here the Metropolis–Hastings Monte Carlo algorithm was used to generate the appropriate statistics of the canonical ensemble that corresponds to the vesicle fluctuating in thermodynamic equilibrium.

2 Inverted hexagonal phase

2.1 Introduction to non-lamellar lipid self-assemblies

It is known that different types of phospholipids that occur in biological organisms may self-assemble into non-lamellar structures if they are extracted from cells and rehydrated in aqueous solution. However, despite the fact that many non-lamellar phases have been undoubtedly identified also in various biological systems [10], still little is understood concerning their function. The induction of non-planar lipid mesophases might play a role in the regulation of protein function. Further, membrane fusion for instance in endo- and exocytosis is thought to be dependent on such highly curved lipid structures [11]. It is also supposed that interbilayer tight junctions host non-bilayer

structures [12, 13]. Last, but not least, lipids forming the non-lamellar structures are indispensable in providing the lipid matrix with special properties, like tuning its flexibility and altering its lateral pressure profile [14], and hence assure the proper function of integral membrane proteins, even in changing environmental conditions [15–17].

The non-lamellar structures of phospholipids are also common in some species of bacteria. It was suggested that the membrane lipid bilayers of bacteria are close to the transition from lamellar to non-lamellar structure [5]. Many different types of bacteria can enzymatically change the intrinsic curvature of phospholipids, consequently, they can prefer the non-lamellar phases [5]. Under laboratory conditions, also higher ordered systems of non-lamellar phases can be prepared such as hexosomes and cubosomes promising applications in nanomedicine [18].

The bicontinuous cubic phases (I*m*3*m*, P*n*3*m*, I*a*3*d*), inverse hexagonal phase (H_{II}) and inverse micellar cubic phase (F*d*3*m*) belong to the biologically most relevant non-lamellar mesophases, Fig. 2. These mesophases resist excess of water and can be stable under certain conditions also in biological systems [19–21]. They can be assembled only from certain kinds of lipids. The most known non-bilayer forming lipids are phosphatidylethanolamines (PEs). They are unique with respect to their headgroup consisted of ethanolamin which is considerably smaller than the tail fatty acid region, (compare Figs. 1 and 2). Their spontaneous shape already prefers the inverse non-bilayer structure. PEs are quite abundant in nature. For example, membrane of *Escherichia coli* contains 70 % of PEs and a great deal of PEs (up to 20 %) can be also found in mitochondrial membranes and red blood cell plasma membranes [22].

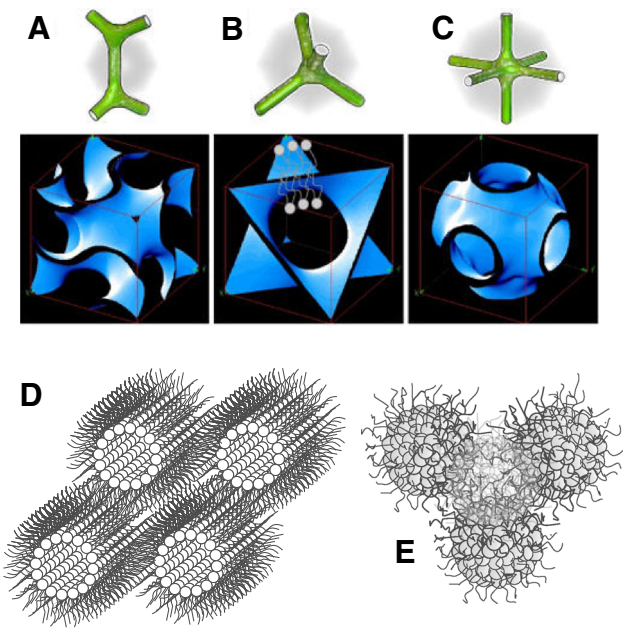

Fig. 2 Schematic figures of non-bilayer self-assemblies: **a–c** bicontinuous cubic phases (adopted from [23]) **d** inverted hexagonal phase and **e** inverse micellar cubic phase

To mathematically describe the non-lamellar inverted hexagonal phase H_{II} we may adopt 2D model which can be easily solved. Two dimensional nature of H_{II} phase offers simple geometry, modelling and numerical calculus. The H_{II}-phase of biomimetic model systems has been intensively studied in order to characterize its geometric and energetic properties [24–27]. Most commonly the bending modulus and intrinsic (spontaneous) radii of different lipid/water systems were evaluated. Note that due to the simple geometry of the H_{II}-phase, a mathematical relationship between the intrinsic shape of the lipid molecules and the given packing frustration can be determined [28, 29].

It is important to note that the commonly used models of the H_{II}-phase assume isotropic lipid intrinsic shapes, and further suppose the polar/apolar interface cross-section to be perfectly circular [30, 31], a simplification that has also been applied in some of our model calculations [25, 32]. According to experimental observations different other models of intrinsic lipid shapes were suggested, such as the sharp hexagonal cross-section. In our present theoretical consideration we further generalized our H_{II}-phase model allowing for deviations of the pivotal plane from a circular cross-section. The pivotal plane is defined as the plane in which the area per lipid molecule is not changed upon applying a bending moment [33, 34]. Indeed, in reality the cross-section of H_{II}-phase is not purely circular, but appears to be hexagon-like with smoothed corners [35–37] (Fig. 3). Although the approximation of circular geometry is sufficient for robust free energy determination of the H_{II}-phase, allowing for deviations from a circular cross-section yields a more accurate evaluation of the lipid membrane material parameters. However, for this it is necessary that the theoretical predictions are compared to highly resolved electron-density maps as available, for instance, for dioleoyl-phosphatidylethanolamine (DOPE) [37].

Recently by Mareš et al. [25] pointed out that by using the concept of the anisotropic shape of lipid molecules may better explain the $L_\alpha - H_{II}$ phase transition and the stability of the H_{II}-phase at higher temperatures than by considering the isotropic lipid shapes only. A similar idea was also expressed earlier [39], but not applied to any model calculations. Hence the model of wedge-like shaped phospholipid molecules was favored over the axisymmetric inverted cone-like model lipid shapes [25, 27] and the corresponding deviatoric energy term averaging the rotational states of the anisotropic compartments was considered [40].

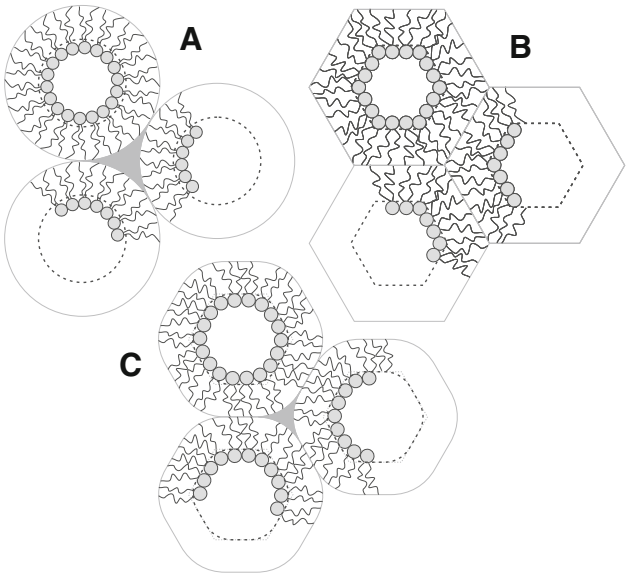

Fig. 3 Schemes of different models of inverted hexagonal phase. **a** Circular cross-section—[30, 31], **b** hexagonal cross-section—[38], **c** intermediate between circular and hexagonal cross-section—[35–37]

2.2 Calculations of the elastic energy of the inverted hexagonal phase by the Monte Carlo simulation

2.2.1 Elastic energy

To calculate the H_{II}-phase optimal geometry by Monte Carlo simulation, we have to first define the free energy of the lipid monolayer in H_{II}-phase. The lipid monolayers in the H_{II}-phase have a strong anisotropic curvature therefore the average orientational ordering of the lipids cannot be neglected. The free energy of a lipid monolayer has been derived [40, 41] starting from the energy of a single molecule and using the methods of statistical physics. The local bending energy of the lipid monolayer in the H_{II}-phase [42] includes the contribution of the deviatoric bending [32, 40] as an additional contribution due to the average orientational ordering of the phospholipids. The whole monolayer free energy is then:

$$F = F_b + F_v \tag{1}$$

where F_b is the monolayer bending energy comprising the anisotropy of lipids and F_v the stretching energy of the lipid chains [25]:

$$F_b = \int_A \frac{n_0\xi}{2}\left((H - H_m)^2 + D^2 + D_m^2\right)dA - n_0 kT \int_A \ln\left(2\cosh\left(\frac{\xi(1+\tilde{k}/kT)D_m D}{kT}\right)\right)dA \tag{2}$$

Here $H = (C_1 + C_2)/2$ is the local mean curvature of the monolayer, $D = |C_1 - C_2|/2$ is the local curvature deviator, $H_m = (C_{1m} + C_{2m})/2$ is the intrinsic mean curvature, $D_m = |C_{1m} - C_{2m}|/2$ is the intrinsic curvature deviator (for details see Ref. [25, 32]), n_0 is the area density of the lipid molecules, ξ is a constant describing the strength of the interaction between a single lipid molecule and the surrounding membrane continuum which is connected to the monolayer bending modulus ($\xi = 2k_c n_0^{-1}$), $\tilde{k}$ is a constant describing the direct interaction between lipid molecules [40], k is the Boltzmann constant, T is temperature and dA is the area element of the monolayer surface. The stretching energy F_v of the lipid chains has the form [25]:

$$F_v = \tau n_0 \int_A (\zeta - \zeta_0)^2 dA. \tag{3}$$

where ζ is the length of the lipid molecule, ζ_0 is the reference length of the molecule and τ is the stretching modulus of the lipid molecule. Considering the H_{II}-phase geometry (Fig. 4), the length of the hydrocarbon chain in polar coordinates may be expressed as:

$$\zeta = \frac{a}{2\cos\varphi} - \rho(\varphi), \tag{4}$$

where a is the unit cell parameter. The aim of our calculations was to obtain the equilibrium contour of the pivotal cross-section represented by the unit cell parameter, a, and the polar coordinates $\rho(\varphi)$ for the different membrane parameters H_m and τ with the constants $k_c = 11\,kT$ [43] for three different lipids; dioleoyl-phosphatidylethanolamine (DOPE), stearoyl-oleoyl-phosphatidylethanolamine (SOPE)

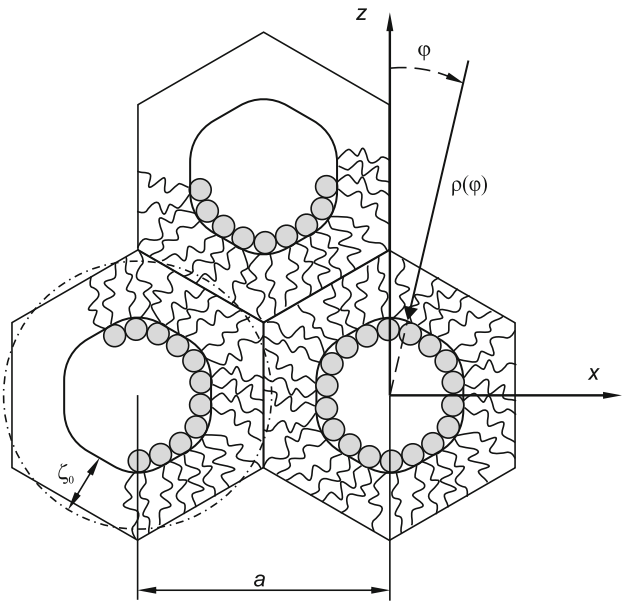

Fig. 4 Cross-section of the H_{II}-phase showing the geometrical parameters: radius vector of the pivotal plane, ρ, unit cell parameter, a, equilibrium length of the hydrocarbon chain, ζ_0, and polar angle, φ. Adopted from [7]

and palmitoyl-oleoyl-phosphatidylethanolamine (POPE). The values of ζ_0 and n_0^{-1} are given in Table 1. Using the definition of the arc length l and the angle ψ leads to expression: $2H = 2D = \mathrm{d}\psi/\mathrm{d}l$ (see Fig. 5). For the sake of simplicity, we consider the anisotropic shape of the lipids at higher temperature as wedge-like, having $C_{2\mathrm{m}} = 0$ and $C_{1\mathrm{m}} < 0$ which yields $H_\mathrm{m} = D_\mathrm{m} = C_{1\mathrm{m}}/2$, [7]. Because of the hexagonal symmetry it is sufficient to determine the equilibrium contour shape for only one twelfth of the pivotal plane cross-section.

2.2.2 Monte Carlo simulated annealing simulations

Equation (1) was minimized numerically by using the Monte Carlo simulated annealing method (MC) [44]. The Monte Carlo simulated annealing method may efficiently find the global minimum of the energy. The contour of the pivotal plane was described by the polar coordinates of radius vector, ρ, and polar angle, $\varphi_i = [0, \pi/6], i = 1, \ldots, N$ which divided a twelfth of the contour line into $N = 60$ points. The starting contour for the MC method was the equilibrium geometry where deviations from circularity were not taken into account (computed as described in Mareš et al. [25]). The boundary conditions were $\psi_{\varphi=0} = 0$ and $\psi_{\varphi=\pi/6} = \pi/6$. In the MC computations ρ_1, ψ_i and a were randomly changed in each step and the energy of the contour was evaluated with respect to the Metropolis criterion, while according to the cooling schedule of simulated annealing $T = (100/(1 + 0.01 \cdot k))$ the temperature parameter was decreased after each step until it reached zero [44]. The number of steps for each computation was 10^7. The radius vector length ρ_i was calculated by using the expression:

$$\rho_{i+1} = \frac{\rho_i(\cos\varphi_i + \sin\varphi_i \tan\psi_i)}{(\cos\varphi_{i+1} + \sin\varphi_{i+1}\tan\psi_i)}. \quad (5)$$

which can be easily derived from the Fig. 5.

The validity of our MC simulation method was tested by variational calculus of the free energy for few different parameters with obtaining an excellent agreement [7].

2.2.3 Results

We obtained the calculated $\mathrm{H_{II}}$-phase contour which corresponds to minimal free energy determined by Monte Carlo simulated annealing method. The results show slight deviations from circularity of the cross-section for given parameters.

Table 1 Values of the optimal (relaxed) length ζ_0 and area per lipid molecule at the pivotal plane $a_0 = n_0^{-1}$ obtained from experiments [25, 37]

	SOPE 68 °C	DOPE 20 °C	POPE 74 °C
ζ_0/nm	1.33	1.20	1.13
n_0^{-1}/nm^2	5.84	5.97	0.65

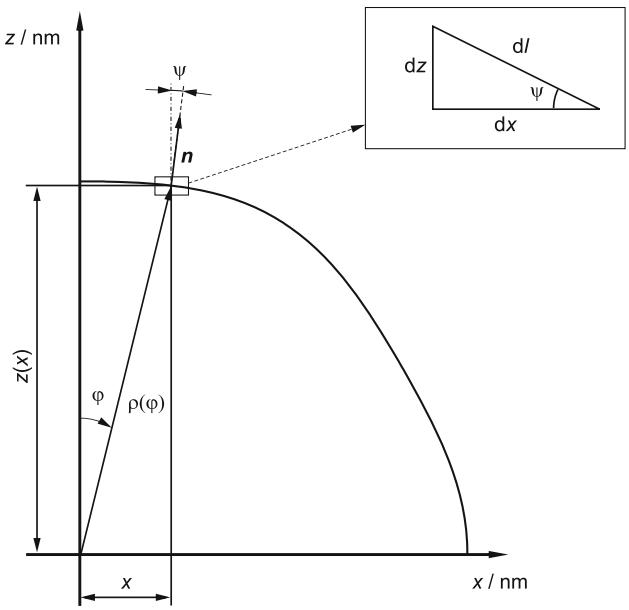

Fig. 5 Illustration of parametrization of the pivotal plane cross-section. The contour is described by Cartesian $z(x)$ and polar $\rho(\varphi)$ coordinates. ψ is the angle between vertical and normal (**n**) in each point. Adopted from reference [7]

The good agreement of the $\mathrm{H_{II}}$-phase pivotal plane cross-section contour shape between experiments and theoretical predictions for both DOPE and SOPE phospholipids can be seen in Figs. 6 and 7, respectively. Good agreement for the pivotal plane cross-section contour was predicted for several combinations of H_m and τ. The range of possible pairs of parameters is restricted to a rather small region in the $H_\mathrm{m}-\tau$ plane. To reproduce a realistic non-circular shape of the pivotal plane which was obtained from experiments τ should not drop below $2kT\,\mathrm{nm}^2$, otherwise even at low temperatures the shape is too circular ($\Delta < 0.5\,\%$) [7]. The upper limit of possible values for τ is restricted by the magnitude of realistic value of the mean radii, which become too small for higher τ. The values of the mean intrinsic curvature H_m are also restricted by the mean radius, namely for higher values of $|H_\mathrm{m}|$ the mean radius is too small to match the experimental contour.

It is obvious that taking into account deviations from circularity slightly lowers the membrane free energy with respect to the case of a purely circular geometry. The decrease is more pronounced for higher deviations from circularity.

It can be concluded that when the hydrocarbon chains are very stiff the membrane must bend towards the hexagon corners in order to help fill the empty parts in hexagon corners. Thus the pivotal plane contour deviates more from

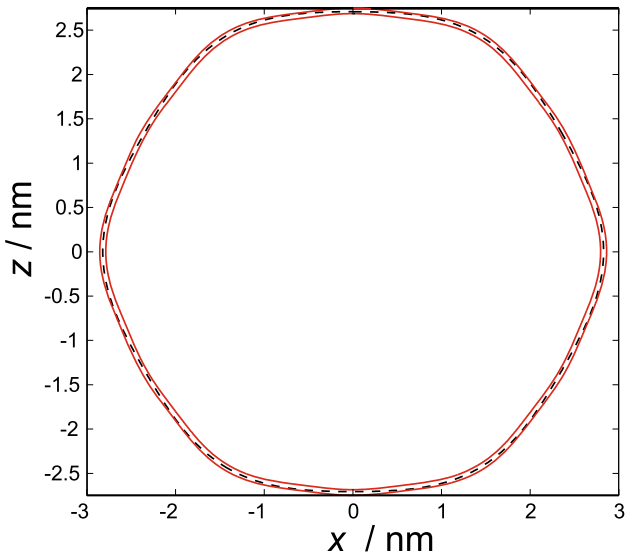

Fig. 6 The best agreement of the experimentally obtained pivotal plane cross-section of DOPE (*full lines*) and theoretical predictions (*dashed line*), where $x = \rho\cos(\varphi)$ and $z = \rho\sin(\varphi)$. The parameters are $H_m = 0.14\ \mathrm{nm}^{-1}$, $\tau = 14.95\,kT\,\mathrm{nm}^{-2}$. Adopted from [7]

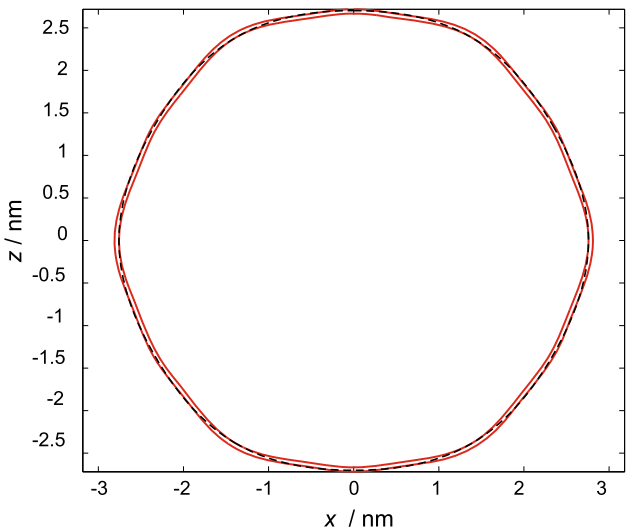

Fig. 7 The best agreement of the experimentally obtained pivotal plane cross-section of SOPE (*full lines*) and theoretical predictions (*dashed line*), where $x = \rho\cos(\varphi)$ and $z = \rho\sin(\varphi)$. The parameters are $H_m = 0.15\ \mathrm{nm}^{-1}$, $\tau = 1.9\,kT\mathrm{nm}^{-2}$. Adopted from [7]

a circle. On the other hand, when the stiffness of the hydrocarbon chain is lower the chains can easily stretch themselves in order to fill the empty parts with keeping the pivotal plane more circular.

In this review, we focussed on the simple two-dimensional inverted hexagonal phase. Nevertheless, there is a possibility to extend the concept for the three-dimensional structures such as hexosomes by taking into account that the axis of the H_{II} cylinder is not straight line with infinite length. This can be done by using the curvilinear coordinates for the axis of the H_{II} cylinder and by addition of the expression for energy of H_{II} cylinder's endings into the free energy. Other three-dimensional task would be solving the stability of bicontinuous cubic phases where some symmetries can be used in order to simplified mathematical description. The anisotropic model of phospholipid molecules, as presented in this manuscript, is also important in bicontinuous cubic phases. Besides the wedge-like molecules the saddle-like molecules with one intrinsic principal curvature negative and the second one positive are important as there are few saddle points in the structure. In this problem, one also should take into account that instead of the monolayer bending energy the bilayer bending energy has to be employed.

3 Monte Carlo simulations of lipid vesicle thermal fluctuations

Cell membranes and lipid bilayers are subject to thermal fluctuations. As for example, the flickering of red blood cells was observed with optical microscopy and reported by Browicz [45]. Cell membrane that separates the interior of the cell from its surroundings is soft and is subjected to water molecules collisions due to their Brownian motion resulting in membrane undulations, which are observed as fluctuations of the shape of the membrane. Spectral analysis of membrane's shape thermal fluctuations can be used to determine elastic properties of the membrane, as we shall discuss below. Experimentally, giant unilamellar lipid vesicles (GUVs) are especially useful for observations of fluctuations, since they have controlled membrane composition and are of the adequate size to be observed under the phase-contrast microscope [46]. Also computer simulations of thermally fluctuating membranes can be applied to explore membrane properties and structure. Using Monte Carlo simulations of nearly spherical lipid vesicles for obtaining elastic properties of vesicle's membrane is the main topic of this section.

3.1 Metropolis–Hastings Monte Carlo algorithm

Models for numerical studies of thermal fluctuations can consider the membranes on atomic level, coarse-grained molecular level, or can take advantage of the high level modelling of the phospholipid bilayer structure and represent the membrane as smoothly curved surface [47].

Phospholipid bilayer membranes can be treated due to its small thickness in first approximation as two dimensional liquid, allowing the continuum approach in the theoretical description of membrane surfaces [47]. In the model presented in this section we discretize the membrane into patches consisting of many molecules. A single patch

is represented by a vertex in a triangulated surface model. The main model parameter that defines mechanical bilayer properties is bending stiffness.

The vesicle is represented by a set of N vertices that are linked by tethers (i.e. bonds) of flexible length d to form a closed, randomly triangulated, self-avoiding network [48, 49]. The lengths of the tethers can vary between a minimal ($d_{\min}$) and a maximal ($d_{\max}$) value. The self-avoidance of the network can be implemented by ensuring that no vertex can penetrate through the triangular network. The maximal possible random displacement of the vertex in a single step (s), should be small enough that the fourth vertex can not move through the plane of the other three to the minimal allowed distance, $d_{\min}$, from the three vertices.

Let us consider the ratio between the maximal and minimal bond lengths, $d_{\max}/d_{\min}$. For $s = 0.15\, d_{\min}$ the self-avoidance constraint gives $d_{\max} < 1.7272\, d_{\min}$. In our simulations we use $s = 0.15\, d_{\min}$ and $d_{\max} = 1.7\, d_{\min}$. For details about the expressions to calculate self-avoidance constraint $d_{\max}$ see [8].

The initial state of triangulated surface is a pentagonal dipyramid with all the edges divided into equilateral bonds so that the network is composed of $3(N-2)$ bonds forming $2(N-2)$ triangles. The system is initially thermalized—evolved into the nearly spherical equilibrium state using same procedure as to acquire the microstates from the simulations. The thermalized structure is shown in Fig. 8.

In our Monte Carlo simulations, the microstates of the vesicle membrane are sampled according to the Metropolis-Hastings algorithm. Evolution of the system is measured in Monte Carlo sweeps (mcs). One mcs consists of individual attempts to displace each of the N vertices by a random increment in the sphere with radius s—the action we will refer to as vertex move. Membrane fluidity is maintained by flipping bonds within the triangulated network. In each mcs, the vertex move attempts are followed by $3N$ attempt to flip a randomly chosen bond. A single bond flip involves the four vertices of two neighboring triangles. The tether between the two vertices is cut and reestablished between the other two, previously unconnected, vertices (see Fig. 9).

Thermal fluctuations of a lipid vesicle in thermodynamic equilibrium are being studied. To obtain the canonical ensemble representing the system in a thermodynamical equilibrium, each individual Monte Carlo step (vertex move or bond flip) is accepted with probability $\min[1, \exp(-\Delta E/kT)]$ according to Metropolis-Hastings algorithm, where ΔE is the energy change due to the vertex move or bond flip.

For the bending energy W_b of the membrane we use the standard Helfrich expression [50] for a tensionless membrane with a zero spontaneous curvature and a fixed topology (the contribution of the Gaussian curvature to the bending energy does not depend on the fluctuations):

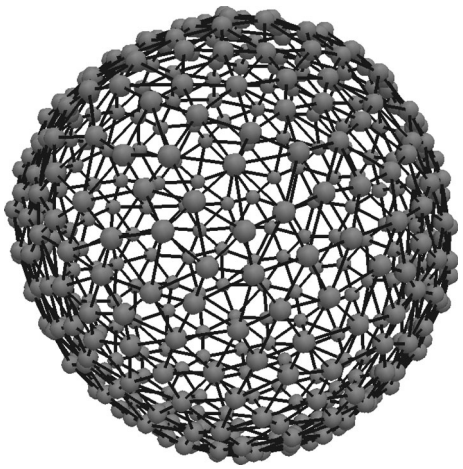

Fig. 8 An example of the triangulated network with $N = 407$ vertices, representing the evolved thermalized structure of the nearly spherical vesicle. The radius of the structure is approximately $7d_{\min}$

$$W_b = \frac{\kappa}{2} \oint_A (c_1 + c_2)^2 \, \mathrm{d}A, \tag{6}$$

where κ is the bending stiffness of the membrane, c_1 and c_2 are the principal curvatures of the vesicle membrane at the point under consideration and the integration is performed over the membrane area A.

For the discretization of the bending energy (Eq. 6) we used the relation [51, 52]

$$\int_A (c_1 + c_2)^2 \, \mathrm{d}A = \sum_i \frac{1}{\sigma_i} \left[\sum_{j(i)} \frac{\sigma_{ij}}{d_{ij}} (\mathbf{R}_i - \mathbf{R}_j) \right]^2, \tag{7}$$

where the outer summation runs over all vertices and the inner summations run over all their nearest neighbors, $\mathbf{R}_i$ is the radial vector of vertex i, d_{ij} is the distance between vertices i and j,

$$\sigma_i = \frac{1}{4} \sum_{j(i)} \sigma_{ij} d_{ij} \tag{8}$$

is the area of the cell in the dual lattice [52] in vertex i. Here $\sigma_{ij} = d_{ij}[\cot(\theta_1) + \cot(\theta_2)]/2$ is the distance between vertices in the dual lattice, θ_1 and θ_2 being opposite angles

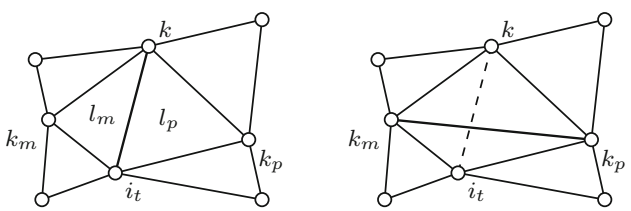

Fig. 9 A bond flip within the triangulated network; this involves the four vertices (i_t, k, k_m and k_p) of the two neighboring triangles (l_m and l_p). The minimal bond (i.e. tether) length is also shown

to side ij in the two triangles that share the common bond ij (see Fig. 10).

The lipid bilayer is on a timescale of thermal fluctuations impermeable for water molecules and due to the low compressibility of water we can assume the vesicle's volume to be constant during thermal fluctuations. The volume of the vesicle in simulations is kept constant at the given value V_0 by the constraint $|V - V_0| < \varepsilon_V$, where ε_V must be small enough to fulfill the condition $\varepsilon_V \ll V_0$, but still not so small to completely suppress the out-of-plane shape fluctuations of the membrane. The choice of ε_V depends on the discretization and is in our work taken to be the volume of the tetrahedron consisting of equilateral triangles with areas A_0/N_t, where A_0 is the area of the spherical vesicle with volume V_0 and N_t is the number of triangles in the triangulated surface:

$$\varepsilon_V = \frac{4\sqrt{2\pi}}{3^{3/4}} \frac{V_0}{N_\mathrm{t}^{3/2}}. \tag{9}$$

With thermal fluctuations some lateral stretching of the membrane occurs on the scale of phospholipid molecules, however, the energy required to significantly change the area of the membrane greatly exceeds the thermal energy kT (product of the Boltzmann constant and the absolute temperature), therefore we can assume that the overall area A of the membrane remains almost constant during thermal fluctuations ($\Delta A \ll A$).

Constant volume and area constraints are required for applying the theory of Milner and Saffran [53] to calculate the bending stiffness of nearly spherical phospholipid vesicles by analyzing the thermally fluctuating shapes of vesicles by decomposing them into spherical harmonics.

3.2 Obtaining elastic properties through spectral analysis of thermal fluctuations in two dimensions

For the sake of simplicity and comparison, we first analyze in details thermal fluctuations of phospholipid vesicles in two dimensions. For a lipid vesicle in three dimensions, the Helfrich bending energy [50] for a membrane with zero spontaneous curvature (symmetric lipid bilayer) and with fixed topology (so the contribution of the Gaussian curvature to the bending energy does not depend on the fluctuations) is described by Eq. 6.

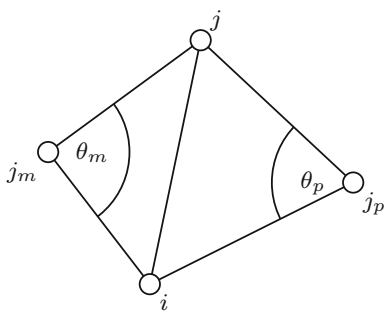

Fig. 10 Part of the network involved in calculation of the distance between vertices in dual lattice σ_{ij}

To make a correspondence with a two-dimensional treatment, imagine a lipid membrane forming a cylinder, namely a bilayer wrapped into a straight tube, long enough that the effects at the both ends of the tube can be neglected. Then one principal curvature is zero and $\mathrm{d}A = h\,\mathrm{d}l$, where h is the cylinder's height and $\mathrm{d}l$ is the length element of the cross-section's contour. We can define $k_\mathrm{c} = h\,\kappa$, with k_c being the two-dimensional analog of the bending stiffness of the membrane with units of energy × length. In this analogy we also have to assume the form of a cylinder for the thermal shape fluctuations. As the lipid bilayer fluctuates, the deviations from a cylinder with a circular cross-section are independent of the coordinate parallel to the cylindrical symmetry axis, or in other words, shape undulations are the same over the whole length of the tube. Another possible analogy is a closed linear polymer of almost circular shape, enclosed in a thin planar film of liquid so that its out of plane fluctuations are completely suppressed. The constant k_c is then $k_\mathrm{c} = kT\,\xi$, where kT is the thermal energy and ξ is the polymer persistence length [8].

Let us consider a nearly circular closed planar curve in the plane that encloses constant area $A = \pi R_0^2$, where R_0 is the radius corresponding to a circle with the same area A. In polar coordinates the curve is described by the radial coordinate $R = R(\varphi, t)$, depending on the polar angle φ and on time t. The bending energy of the curve can then be written as

$$W_\mathrm{b} = \frac{1}{2} k_\mathrm{c} \oint_{L(t)} C^2\,\mathrm{d}l = \frac{1}{2} k_\mathrm{c} \int_0^{2\pi} C^2 \sqrt{R^2 + R'^2}\,\mathrm{d}\varphi, \tag{10}$$

with curvature $C = C(\varphi, t)$ and the element of contour length $\mathrm{d}l = \sqrt{R^2 + R'^2}\,\mathrm{d}\varphi$ of the closed curve with total length $L = L(t)$. Note that curvature C, radial coordinate R and contour length in general all change with time t due to thermal fluctuations. We use the prime symbol for denoting the operator of the first partial derivative with respect to φ. Similarly we use the double prime symbol for denoting the second partial derivative with respect to φ. In polar coordinates the curvature C can then be written as

$$C = \frac{R^2 + 2R'^2 - RR''}{\left(R^2 + R'^2\right)^{3/2}}. \tag{11}$$

Note that the constant k_c in Eq. 10 has units of energy × length and represents the "two-dimensional" bending stiffness [8].

For the circle with radius R_0, Eq. 10 yields the bending energy

$$W_0 = \frac{1}{2}k_c \int_0^{2\pi} \frac{1}{R_0^2} R_0 \, d\varphi = \frac{\pi k_c}{R_0}. \tag{12}$$

Consider the relative deviations, $r = r(\varphi, t)$, from the circle with radius R_0,

$$R(\varphi, t) = R_0(1 + r(\varphi, t)). \tag{13}$$

Then we can express the squared curvature, which we will need for calculating the bending energy (from Eq. 10) as

$$C^2 = \frac{[1 + 2r + r^2 + 2r'^2 - (1 + r)r'']^2}{R_0^2 [(1 + r)^2 + r'^2]^3}. \tag{14}$$

Now we assume that thermal fluctuation do not cause too much deviation of the contour from a circular shape. More specifically, we assume that the relative deviations from a circle and its first and second derivatives with respect to φ are small:

$$r(\varphi, t) \ll 1, \tag{15}$$

$$r'(\varphi, t) \ll 1, \tag{16}$$

$$r''(\varphi, t) \ll 1. \tag{17}$$

Therefore we can expand C^2 (from Eq. 14) up to the second order in r, r', r'' to get

$$C^2 = \frac{3r^2 + r'^2 + (r'' - 1)^2 + r(6r'' - 2)}{R_0^2}. \tag{18}$$

Expanding the length element,

$$dl = \sqrt{R^2 + R'^2}\, d\varphi = R_0 \left(1 + r + \frac{r'^2}{2}\right) d\varphi, \tag{19}$$

the bending energy from Eq. 10 becomes

$$W_b = \frac{k_c}{2R_0} \int_0^{2\pi} \left[r^2 + \frac{3}{2}r'^2 + (r'' + 1)^2 + r(4r'' - 1)\right] d\varphi. \tag{20}$$

Further, the relative deviations from a circle are expended into the Fourier series:

$$r(\varphi, t) = \sum_{n=-n_{max}}^{n_{max}} z_n(t) e^{in\varphi}, \tag{21}$$

where the cutoff $n_{max} \sim R_0/\lambda_{mol}$ is introduced, with λ_{mol} is typical intramolecular distance. For brevity the limits are omitted in the summation signs in all expressions below [8].

Note that the complex amplitudes have the property $z_{-n}(t) = z_n^*(t)$, assuring that relative deviations $r(\varphi, t)$ are real numbers. The first and the second derivatives with respect to φ are then

$$r'(\varphi, t) = i \sum_{n=-n_{max}}^{n_{max}} n\, z_n(t) e^{in\varphi}, \tag{22}$$

$$r''(\varphi, t) = -\sum_{n=-n_{max}}^{n_{max}} n^2 z_n(t) e^{in\varphi}. \tag{23}$$

Inserting the above expressions 22 and 23 into Eq. 20, and performing integration over the polar angle φ, we can get

$$\int_0^{2\pi} r \, d\varphi = \sum_n z_n \int_0^{2\pi} e^{in\varphi} d\varphi = 2\pi z_0, \tag{24}$$

$$\int_0^{2\pi} r^2 \, d\varphi = \sum_{n,m} z_n z_m \int_0^{2\pi} e^{i(n+m)\varphi} d\varphi = 2\pi \sum_n |z_n|^2 \tag{25}$$

and similarly

$$\int_0^{2\pi} r'^2 \, d\varphi = 2\pi \sum_n n^2 |z_n|^2, \tag{26}$$

$$\int_0^{2\pi} r'' \, d\varphi = -\sum_n n^2 z_n \int_0^{2\pi} e^{in\varphi} d\varphi = 0, \tag{27}$$

$$\int_0^{2\pi} r''^2 \, d\varphi = 2\pi \sum_n n^4 |z_n|^2, \tag{28}$$

$$\int_0^{2\pi} r r'' \, d\varphi = -2\pi \sum_n n^2 |z_n|^2. \tag{29}$$

Therefrom we obtain $\Delta W_b = W_b - W_0$, where $W_0 = \pi k_c / R_0$ (see Eq. 12) is the bending energy of the circle with radius R_0,

$$\Delta W_b = \frac{\pi k_c}{R_0} \left[-z_0 + \sum_n \left(n^4 - \frac{5}{2}n^2 + 1\right) |z_n|^2\right]. \tag{30}$$

The zero-mode amplitude z_0 can be expressed using the equation of area conservation $A = \pi R_0^2$. Taking into account

$$A = \int_0^{2\pi} \frac{R^2}{2} d\varphi = \pi R_0^2 \left[1 + 2z_0 + \sum_n |z_n|^2\right] \tag{31}$$

we see

$$z_0 = -\frac{1}{2} \sum_n |z_n|^2 \tag{32}$$

and therefore the expression for the bending energy is

$$\Delta W_{\mathrm{b}}(t) = \frac{\pi k_{\mathrm{c}}}{R_0} \sum_{n \neq 0} \left(n^4 - \frac{5}{2} n^2 + \frac{3}{2} \right) |z_n(t)|^2, \tag{33}$$

where n in the summation runs over all nonzero integers from $-n_{\max}$ to $n_{\max}$. The term $|z_0|^2$ is not taken into account in the above summation, since it is of the fourth order in the amplitudes z_n, as seen from Eq. 32.

The total elastic energy of our fluctuating closed contour is the sum of the bending contribution (Eq. 33) and the stretching contribution. The stretching energy can be represented as

$$W_{\mathrm{s}}(t) = \oint_{L(t)} \frac{1}{2} \frac{[\lambda(t)]^2}{k_{\mathrm{s}}} \, \mathrm{d}l_{\mathrm{r}} = \frac{1}{2} \frac{[\lambda(t)]^2}{k_{\mathrm{s}}} L_{\mathrm{r}}, \tag{34}$$

where k_{s} is the "stretching modulus" (with units of energy $\times$ length), $L = L(t)$ is the contour length,

$$\lambda(t) = k_{\mathrm{s}} \frac{L(t) - L_{\mathrm{r}}}{L_{\mathrm{r}}} \tag{35}$$

is the tension and L_{r} is the tension-free contour length (relaxed membrane). Let us note that tension $\lambda = \lambda(t)$ fluctuates with time t, but can be taken as constant along the contour (or vesicle membrane in 3D) [54]. The reason why the integral in Eq. 34 runs over the length element $\mathrm{d}l_{\mathrm{r}}(t)$ of the tension-free membrane (and not, say, $\mathrm{d}l(t)$) lies in the fact that $\mathrm{d}l_{\mathrm{r}}(t)$ is proportional to the number of molecules in the length $\mathrm{d}l(t)$ and that what we calculate is the energy per molecule (or, in other words, energy for the part of the membrane with a fixed number of molecules in it) [8].

Introducing the time averaged tension as

$$\langle \lambda \rangle = k_{\mathrm{s}} \frac{\langle L \rangle - L_{\mathrm{r}}}{L_{\mathrm{r}}}, \tag{36}$$

and using the relation

$$\lambda(t) - \langle \lambda \rangle = k_{\mathrm{s}} \frac{L(t) - \langle L \rangle}{L_{\mathrm{r}}}, \tag{37}$$

we can rewrite the stretching energy from Eq. 34 as:

$$\begin{aligned} W_{\mathrm{s}}(t) &= \frac{1}{2} k_{\mathrm{s}} \frac{[L(t) - L_{\mathrm{r}}]^2}{L_{\mathrm{r}}} \\ &= \frac{1}{2} k_{\mathrm{s}} \frac{[L(t) - \langle L \rangle + \langle L \rangle + L_{\mathrm{r}}]^2}{L_{\mathrm{r}}} \\ &= \langle \lambda \rangle [L(t) - \langle L \rangle] + \frac{L_{\mathrm{r}} \langle \lambda \rangle^2}{2 k_{\mathrm{s}}} \\ &\quad + \frac{1}{2} [\lambda(t) - \langle \lambda \rangle][L(t) - \langle L \rangle]. \end{aligned} \tag{38}$$

Note that in the second line of the expression 38 the second term is the stretching energy of the contour with the average length $\langle L \rangle$ is independent of time. We define

$$\begin{aligned} \Delta W_{\mathrm{s}}(t) &= \langle \lambda \rangle [L(t) - L_0] \\ &\quad + \frac{1}{2} [\lambda(t) - \langle \lambda \rangle][L(t) - \langle L \rangle] + const., \end{aligned} \tag{39}$$

where the constant term does not depend on time and $L_0 = 2\pi R_0$ is the contour length of the circle with area A. It can be seen that

$$L(t) - L_0 = \oint_{L(t)} \mathrm{d}l - L_0 = \pi R_0 \sum_{n \neq 0} (n^2 - 1) |z_n(t)|^2 \tag{40}$$

and that

$$L(t) - \langle L \rangle = \pi R_0 \sum_{n \neq 0} \left\{ (n^2 - 1) \left[|z_n(t)|^2 - \left\langle |z_n(t)|^2 \right\rangle \right] \right\}. \tag{41}$$

Therefore the second term in Eq. 39 is the product of the fluctuations of the molecular (mean) field (namely, $[\lambda(t) - \langle \lambda \rangle]$, created by the squares $|z_n(t)|^2$ of the amplitudes of all modes available) and the fluctuations of the square $\left[|z_n(t)|^2 - \langle |z_n(t)|^2 \rangle \right]$ of the amplitude of the mode under consideration. The main idea of the mean-field approximation is to disregard the correlations of the molecular field with fluctuations of its conjugated quantity. Therefore the second term in Eq. 39 is omitted and this gives us

$$\begin{aligned} \Delta W(t) &= \Delta W_{\mathrm{b}}(t) + \Delta W_{\mathrm{s}}(t) \\ &= \frac{\pi k_{\mathrm{c}}}{R_0} \sum_{n \neq 0} (n^2 - 1) \left(n^2 + \bar{\lambda} - \frac{3}{2} \right) |z_n(t)|^2 \\ &\quad + const., \end{aligned} \tag{42}$$

where we introduced the dimensionless average tension $\bar{\lambda} = \langle \lambda \rangle R_0^2 / k_c$.

Performing the time averaging of the above expression and taking into account the equipartition theorem that each fluctuation mode on the average contributes $k_{\mathrm{B}}T/2$ to the energy, we finally obtain the expression for the mean squared amplitudes:

$$\left\langle |z_n|^2 \right\rangle = \frac{kT}{2} \frac{R_0}{\pi k_{\mathrm{c}}} \frac{1}{(n^2 - 1)\left(\bar{\lambda} + n^2 - \frac{3}{2} \right)}. \tag{43}$$

The mean squared amplitudes for the modes $n \geq 2$ diverge for negative values of the lateral tension, as expected ($\langle |z_2|^2 \rangle$ diverges for $\bar{\lambda} = -2.5$) [8].

3.3 The determination of elastic properties of lipid bilayer vesicle through spectral analysis of thermal fluctuations in three dimensions

Similar expression as the above Eq. 43 for two dimensions was derived for three dimensions by Milner and Safran [53]. Their theory allows us to obtain the bending stiffness

K_c of the membrane from the spectral analysis of thermal fluctuations of the nearly spherical vesicle. In this section we apply the theory of Milner and Safran on our randomly triangulated surfaces simulations. Note that the bending stiffness κ is an input parameter in our simulations and that we used a different symbol (K_c) for the bending stiffness obtained from the spectral analysis of thermal fluctuations (in two dimensional case, the symbol k_c was used). From now on, to distinguish the two values κ and K_c, we name them the *input* bending stiffness and the *measured* bending stiffness, respectively.

Consider now triangulated nearly spherical vesicle with volume V_0 and let R_0 be the radius of a sphere with the same volume. The length of the radial vector $R_i(t) = R(\vartheta_i, \varphi_i, t)$ from the origin to the vertex i at time t is then defined as

$$R(\vartheta_i, \varphi_i, t) = R_0[1 + r(\vartheta_i, \varphi_i, t)], \tag{44}$$

where ϑ_i and φ_i are the spherical coordinates of the ith vertex and $r(\vartheta_i, \varphi_i, t)$ is the relative displacement of the ith vertex [9].

Relative displacements $r(\vartheta_i, \varphi_i, t)$ are decomposed into a series with respect to the spherical harmonics $Y_l^m(\vartheta_i, \varphi_i)$:

$$r(\vartheta_i, \varphi_i, t) = \sum_{l=0}^{l_{\max}} \sum_{m=-l}^{l} u_l^m(t) Y_l^m(\vartheta_i, \varphi_i), \tag{45}$$

where cutoff $l_{\max}$ is of the order of $R_0/d_{\min}$ and the spherical harmonics are defined as

$$Y_l^m(\vartheta, \varphi) = \sqrt{\frac{(2l+1)}{4\pi}\frac{(l-m)!}{(l+m)!}} P_l^m\big(\cos(\vartheta)\big) \mathrm{e}^{im\varphi} \tag{46}$$

using associated Legendre polynomials P_l^m [9].

The complex coefficients $u_l^m(t)$ can then be calculated using the relation

$$u_l^m(t) = \int_\Omega r(\vartheta, \varphi, t) \big(Y_l^m(\vartheta, \varphi)\big)^* \mathrm{d}\Omega, \tag{47}$$

where the integration runs over the solid angle Ω of the sphere. The discretization of the above expression can be done as

$$u_l^m(t) = \sum_{i=1}^{N} \Omega_i(t) r_i(t) \big(Y_l^m(\vartheta_i(t), \varphi_i(t))\big)^*, \tag{48}$$

where $\Omega_i(t)$ is the solid angle corresponding to vertex i and the sum runs over all vertices of the triangulated surface [9].

The mean squared amplitudes of spherical harmonics $\langle |u_l^m|^2 \rangle$ are calculated by averaging the $|u_l^m(t)|^2$ values over an ensemble of microstates of the vesicle in the thermal equilibrium. Using the expression of Milner and Safran [53],

$$\left\langle |u_l^m|^2 \right\rangle = \frac{kT}{K_c} \frac{1}{(l-1)(l+2)(\bar{\sigma} + l(l+1))}, \tag{49}$$

the bending stiffness K_c and the dimensionless mean lateral tension $\bar{\sigma}$ of the membrane can be obtained.

Since the rhs of Eq. 49 do not depend on the order of spherical harmonics m, the mean squared amplitudes of spherical harmonics obtained from simulations are first averaged over m and then the obtained values $\langle |u_l|^2 \rangle$ are used on the lhs of Eq. 49:

$$\left\langle |u_l|^2 \right\rangle = \frac{kT}{K_c} \frac{1}{(l-1)(l+2)(\bar{\sigma} + l(l+1))}. \tag{50}$$

To obtain the bending stiffness K_c and the dimensionless mean lateral tension $\bar{\sigma}$ of the membrane together with their standard errors, the $\langle |u_l|^2 \rangle$ from simulations are fitted with the formula of Milner and Safran (Eq. 50) using an inverse squared variance weighted nonlinear fit [9].

3.4 Results and discussion

For each set of parameters the system is initially thermalized into a nearly spherical vesicle and then the volume is fixed. The squared amplitudes of spherical harmonics $|u_l^m|^2$ are obtained from Monte Carlo simulations as described in Sect. 3.3.

To obtain the ensemble of microstates that are statistically independent, the autocorrelations of squared amplitudes $f(|u_l^m|^2, \tau)$ are calculated with the autocorrelation function

$$f(x, \tau) = \frac{\sum_{t=1}^{T-\tau} (x(t) - \langle x \rangle)(x(t+\tau) - \langle x \rangle)}{\sum_{t=1}^{T-\tau} (x(t) - \langle x \rangle)^2}, \tag{51}$$

where the sums run over the discrete "time" t denoting consecutive microstates and T is the number of microstates used in the calculation of the mean $\langle x \rangle$. Let us define the decay time of $|u_l^m|^2$ as the value of τ when the autocorrelation function $f(|u_l^m|^2, \tau)$ falls bellow 1/e.

Figure 11 shows the autocorrelation functions of the few lowest relevant modes for a system with $N = 1127$ vertices and input bending stiffness $\kappa = 20\,kT$. It can be seen that the longest decay times are for $|u_2^m|^2$ i.e. the decay time decreases with the increasing degree of the spherical harmonics l, as expected. Let us denote the largest decay time of all the relevant modes for a given system with N vertices as τ_N (in Fig. 11 we have $\tau_{1127} \approx 60{,}000$). The largest decay time τ_N decreases with the increasing input bending stiffness κ, while it increases with the number of vertices N in the triangulated network.

The decay time τ_N is important for our spectral analysis since it can be used to estimate the "time" interval between two microstates that can be regarded as statistically uncorrelated. The ensemble of statistically uncorrelated

states is needed for the estimation of the standard errors together with the means of squared amplitudes of spherical harmonics. Those standard errors of $\langle|u_l^m|^2\rangle$ have to be taken into account in the fitting procedure in Eq. 50, to obtain relevant values of the bending stiffness K_c and the dimensionless mean lateral tension $\bar{\sigma}$ of the membrane. The interval between two consecutive microstates in an ensemble of statistically uncorrelated states, i.e. between two consecutive "measurements", was always larger than three times the largest decay time τ_N. In Fig. 11, for example, the x-axis spans the "time" interval between consecutive measurements for a system with $N = 1127$ and $\kappa = 20\,kT$.

When squared amplitudes $|u_l^m|^2$ are averaged over the ensemble of microstates, the obtained $\langle|u_l^m|^2\rangle$ with the same order m converge towards the same value, as shown in Fig. 12 for $|u_2^m|^2$. This is in accordance with the theory of Milner and Safran (rhs of Eq. 49 are independent of m). Also Fig. 13 shows that the mean squared amplitudes obtained from simulations are independent of m. Note that our previously reported [8] inability to observe this independence of $\langle|u_l^m|^2\rangle$ on m was a result of numerical errors.

The measured bending stiffness K_c and the dimensionless mean lateral tension $\bar{\sigma}$ are obtained from the mean squared amplitudes as described in Sect. 3.3. The result of a fitting procedure for K_c is shown in Fig. 14 as a function of the maximal degree l of spherical harmonics used in the fitting of $\langle|u_l|^2\rangle$ in Eq. 50 (Eqs. for all values from $l = 2$ up to the maximal degree l are taken into account).

The measured bending stiffness K_c is shown in Fig. 15 as a function of the number of vertices N of the triangulated surface. As expected, the difference between the measured bending stiffness K_c and the input bending stiffness $\kappa = 20\,kT$ decreases as we increase the number of vertices in the triangulation (i.e. as we increase the resolution of the discretization).

Figure 15 also shows the obtained values of the dimensionless mean lateral tension $\bar{\sigma}$ for the same sets of measurements. Let us note that the measured values of K_c should not depend on the value of $\bar{\sigma}$. The mean lateral tension in the membrane depends on the value of the fixed volume of the vesicle, i.e. how much the vesicle is "swollen". This is somewhat arbitrarily chosen by picking a random microstate in the thermodynamical equilibrium when fixing the volume and starting the measuring procedure for K_c and $\bar{\sigma}$. As expected, the exact choice of the equilibrium microstate used when fixing the volume, i.e. the value of $\bar{\sigma}$, does negligibly influence the measured K_c.

Figure 16 shows the relative difference between the measured and the input bending stiffness, $K_c/\kappa - 1$, for different values of the input bending stiffness κ. It can be seen that increasing the input bending stiffness decreases the mismatch between the input and the measured bending stiffness. Note that, as already reported above, the correlation times of squared amplitudes decrease with the increasing bending stiffness of the membrane.

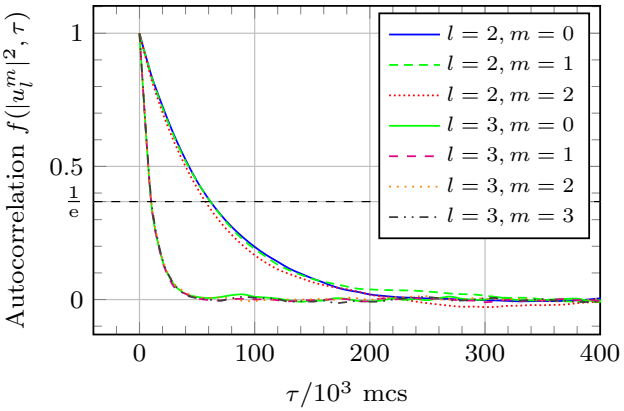

Fig. 11 Autocorrelation functions $f(|u_l^m|^2, \tau)$ of the lowest relevant degrees of spherical harmonics $l = 2$ and $l = 3$, for $N = 1127$ and $\kappa = 20\,kT$. The *dashed gray horizontal line* indicates the value 1/e. The decay time of a given mode is defined as time when the autocorrelation function falls below this value [9]

4 Conclusions

In this section we presented two Monte Carlo methods applied to phospholipid systems.

We solved the stability of inverted hexagonal phase by minimizing the free energy of the lipid monolayer by Monte Carlo simulated annealing method. It is an example of using the stochastic method instead of the variational calculus or other analytical methods and more effective then methods using different kinds of approximations. The next step could be to model three-dimensional bicontinuous phases and their stability.

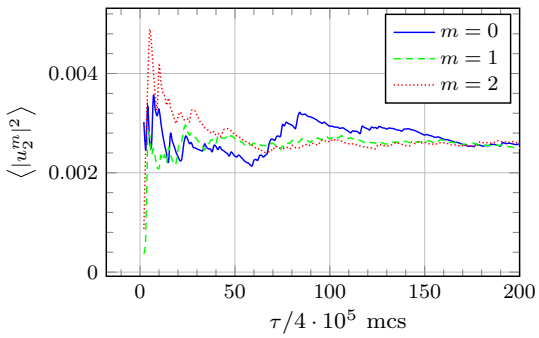

Fig. 12 Mean squared amplitudes $\langle|u_2^0|^2\rangle$ (*full*), $\langle|u_2^1|^2\rangle$ (*dashed*) and $\langle|u_2^2|^2\rangle$ (*dotted*) as a function of the number of statistically independent measurements used in the averaging. The input bending stiffness $\kappa = 20\,kT$ and the membrane is triangulated with $N = 1127$ vertices [9]

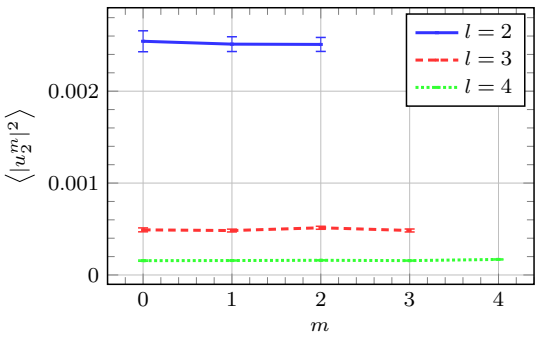

Fig. 13 Mean squared amplitudes $\langle |u_l^m|^2 \rangle$ for $l = 2$, 3 and 4, obtained from 1000 measurement for a vesicle with input bending stiffness $\kappa = 20\,kT$ and triangulated with $N = 1127$ vertices. The *error bars* indicate the standard error (standard deviation divided by the square-root of the number of measurements). *Lines* connect the points with the same degree l and are for the guide-of-eye only. Adapted from [9]

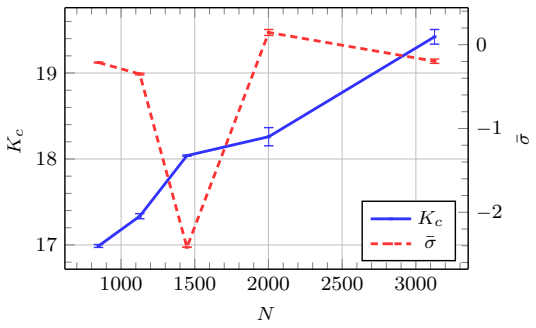

Fig. 15 Measured bending stiffness K_c together with standard error (*error bars*) as a function of the number of vertices N used in the triangulation of the membrane, for the input bending stiffness $\kappa = 20\,kT$. The dimensionless mean lateral tension $\bar{\sigma}$ for the same sets of measurements is also shown. *Lines* connecting the points are for the guide-of-eye only. Adapted from [9]

We also presented Monte Carlo simulations of thermal fluctuations of phospholipid vesicle and its analysis for obtaining membrane's elastic properties [9]. The theoretical basis of this analysis, proposed by Milner and Safran [53], uses the mean field approximation. In the presented work, the error of the determination of the bending stiffness due to the approximations used in the theory was estimated.

Monte Carlo simulations of the fluctuating nearly spherical lipid vesicle have been performed using randomly triangulated surface. The time mean squares of the amplitudes of the fluctuations, obtained from the simulations, can be determined with an arbitrarily high precision, depending only on the length of the simulation. One of the parameters in the simulations is the input value of the bending stiffness. The obtained time mean squares of the amplitudes of the fluctuations are considered as experimental values, which are then used for the determination of the output value of the bending stiffness by means of the theory of Milner and Safran. The presented theory would be "exact" if the output value of the bending stiffness would have been equal to the input one. Our results show that the difference between the two values of the bending stiffness decreases with the increase of the resolution of the triangulated network and can be well below 10 %.

Therefore, we can conclude that the theory of Milner and Safran can be successfully used in the determination of the bending stiffness of the membrane of a nearly spherical lipid vesicle. According to our results, the errors due to the approximations adopted in the theory are less than 10 %.

The analysis of the Monte Carlo simulations of thermal fluctuations of phospholipid vesicles can also be a useful tool to predict the change of the bending stiffness of biological membranes due to their chemical modification. Altering the properties of the triangulated surface and/or introducing other membrane-interacting objects in the simulations, and then measure the change of the bending

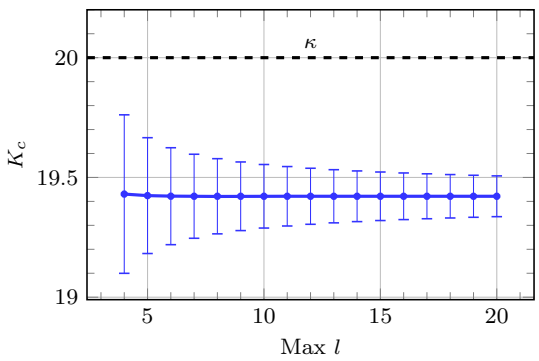

Fig. 14 Measured bending stiffness K_c together with standard error (*error bars*) as a function of the maximal degree l of spherical harmonics used in the calculation of K_c and $\bar{\sigma}$. The value of the input bending stiffness $\kappa = 20\,kT$ is indicated with a *horizontal dashed line*. The membrane is triangulated with $N = 3127$ vertices and 200 statistically independent microstates are measured (between each measured microstate is an interval of 2×10^6 mcs). *Lines* connecting the points are for the guide-of-eye only. Adapted from [9]

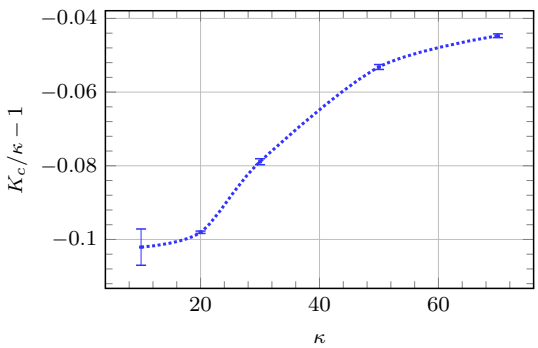

Fig. 16 Relative difference between the measured and the input bending stiffness as a function of the input bending stiffness for the membrane triangulated with $N = 1447$ vertices. Adapted from [9]

stiffness, offers many useful applications. Multicomponent lipid bilayers, membranes decorated with inclusions like peptides, polymer coated vesicles like PEGylated or polyelectrolyte-grafted vesicles.

References

1. Alberts, B., Johnson, A., Lewis, J., Raff, M., Roberts, K., Walter, P.: Molecular Biology of the Cell, 4th edn. Garland Science, New York (2002)
2. Cooper, G.M.: The Cell—A Molecular Approach, 2nd edn. Sinauer Associates, Sunderland (MA) (2000)
3. Berg, J.M., Tymoczko, J.L., Stryer, L.: Biochemistry, 5th edn. W H Freeman, San Francisco (2002)
4. Mouritsen, O.: Life—As a Matter of Fat: The Emerging Science of Lipidomics. The Frontiers Collection. Springer, Berlin (2004)
5. Mouritsen, O.G.: Life—As a Matter of Fat. Springer, Berlin (2005)
6. Seddon, J., Templer, R.: Liquid crystals and the living cell. New Sci. **130**, 45–49 (1991)
7. Perutková, v, Daniel, M., Rappolt, M., Pabst, G., Dolinar, G., Kralj-Iglič, V., Iglič, A.: Elastic deformations in hexagonal phases studied by small-angle X-ray diffraction and simulations. Phys. Chem. Chem. Phys. **13**, 3100–3107 (2011)
8. Fošnarič, M., Penič, S., Iglič, A., Bivas, I.: Chapter twelve—Thermal fluctuations of phospholipid vesicles studied by Monte Carlo simulations. In: Iglič, A., Genova, J. (eds.) Advances in Planar Lipid Bilayers and Liposomes. Advances in Planar Lipid Bilayers and Liposomes, vol. 17, pp. 331–357. Academic Press (2013). doi:10.1016/B978-0-12-411516-3.00012-7
9. Penič, S., Iglič, A., Bivas, I., Fošnarič, M.: Bending elasticity of vesicle membranes studied by Monte Carlo simulations of vesicle thermal shape fluctuations. Soft Matter **11**, 5004–5009 (2015). doi:10.1039/C5SM00431D
10. Hyde, S., Anderson, S., Larsson, K., Blum, Z., Landth, T., Lidin, S., Ninham, B.: The Language of Shape. Elsevier, Amsterdam (1997)
11. Jahn, R., Lang, T., Südhof, T.: Membrane fusion. Cell **112**, 519–533 (2003)
12. Hui, S., Stewart, T., Boni, L., Yeagle, P.L.: Membrane fusion through point defects in bilayers. Science **212**, 921–923 (1981)
13. Siegel, D.: The modified stalk mechanism of lamellar/inverted phase transitions and its implications for membrane fusion. Biophys. J. **76**, 291–313 (1999)
14. Jerabek, H., Pabst, G., Rappolt, M., Stockner, T.: Membrane-mediated effect on ion channels induced by the anesthetic drug ketamine. J. Am. Chem. Soc. **132**, 7990–7997 (2010)
15. Gruner, S.: Intrinsic curvature hypothesis for biomembrane lipid composition: a role for nonbilayer lipids. Proc. Natl. Acad. Sci. USA **82**, 3665–3669 (1985)
16. de Kruijff, B.: Lipid polymorphism and biomembrane function. Curr. Opin. Chem. Biol **1**, 564–569 (1997)
17. Zimmerberg, J., Kozlov, M.: How proteins produce cellular membrane curvature. Nat. Rev. **7**, 9–19 (2006)
18. Boyd, B., Rizwan, S., Dong, Y.D., Hook, S., Rades, T.: Self-assembled geometric liquid-crystalline nanoparticles imaged in three dimensions: Hexosomes are not necessarily flat hexagonal prisms. Langmuir **23**, 12461–12464 (2007)
19. Luzzati, V.: Biological significance of lipid polymorphism: the cubic phases. Curr. Opin. Struct. Biol. **7**, 661–668 (1997)
20. Luzzati, V., Tardieu, A., Gulik-Krzywicki, T., Rivas, E., Reiss-Husson, F.: Structure of the cubic phases of lipid water systems. Nature **220**, 485–488 (1968)
21. Rappolt, M.: Advances in planar lipid bilayer and liposomes. In: Leitmannova Liu, A. (ed.) The Biologically Relevant Lipid Mesophases as "Seen" by X-rays, pp. 253–283. Academic Press, Burlington (2006)
22. Alberts, B., Johnson, A., Lewis, J., Raff, M., Roberts, K., Walter, P.: Molecular Biology of the Cell. Garland Science, New York (2008)
23. Yaghmur, A., Laggner, P., Zhang, S., Rappolt, M.: Tuning curvature and stability of monoolein bilayers by designer lipid-like peptide surfactants. PLoS ONE **2**, e479 (2007)
24. Harper, P., Mannock, D., Lewis, R., McElhaney, R., Gruner, S.: X-ray diffraction structures of some phosphatidylethanolamine lamellar and inverted hexagonal phases. Biophys. J. **81**, 2693–2706 (2001)
25. Mareš, T., Daniel, M., Perutková, Š., Perne, A., Dolinar, G., Iglič, A., Rappolt, M., Kralj-Iglič, V.: Role of phospholipid asymmetry in the stability of inverted hexagonal mesoscopic phases. J. Phys. Chem. B **112**, 16575–16584 (2008)
26. Rappolt, M., Hickel, A., Bringezu, F., Lohner, K.: Mechanism of the lamellar/inverse hexagonal phase transition examined by high resolution X-ray diffraction. Biophys. J. **84**, 3111–3122 (2003)
27. Rappolt, M., Hodzic, A., Sartori, B., Ollivon, M., Laggner, P.: Conformational and hydrational properties during the l_β to l_α- and l_α- to h_{ii}-phase transition in phosphatidylethanolamine. Chem. Phys. Lipids **154**, 46–55 (2008). doi:10.1016/j.chemphyslip.2008.02.006
28. Churchward, M., Rogasevskaia, T., Brandman, D., Khosravani, H., Nava, P., Atkinson, J., Coorssen, J.: Specific lipids supply critical negative spontaneous curvature–an essential component of native Ca^{2+}-triggered membrane fusion. Biophys. J. **94**, 3976–3986 (2008)
29. Kozlov, M.: Determination of lipid spontaneous curvature from X-ray examinations of inverted hexagonal phases. Methods Mol. Biol. **400**, 355–366 (2007)
30. Rand, R., Fuller, N., Gruner, S., Parsegian, V.: Membrane curvature, lipid segregation, and structural transitions for phospholipids under dual-solvent stress. Biochemistry **29**, 76–87 (1990)
31. Siegel, D.: Energetics of intermediates in membrane fusion:-comparison of stalk and inverted micellar intermediate mechanisms. Biophys. J. **65**, 2124–2140 (1993)
32. Perutková, Š., Daniel, M., Dolinar, G., Rappolt, M., Kralj-Igli/vc, V., Iglič, A.: Advances in planar lipid bilayers and liposomes. In: Leitmannova Liu A. (ed.) Stability of the Inverted Hexagonal Phase, vol. 9, pp. 237–278. Academic Press, Burlington (2009)
33. KozIov, M., Leikin, S., Rand, R.: Bending, hydration and interstitial energies quantitatively account for the hexagonal-lamellar-hexagonal reentrant phase transition in dioleoylphosphatidylethanolamine. Biophys. J. **67**, 1603–1611 (1994)
34. Leikin, S., Kozlov, M.M., Fuller, N.L., Rand, R.P.: Measured effects of diacylglycerol on structural and elastic properties of phospholipid membranes. Biophys. J. **71**, 2623–2632 (1996)
35. Malinin, V., Lentz, B.: On the analysis of elastic deformations in hexagonal phases. Biophys. J. **86**(5), 3324–3328 (2004). doi:10.1016/S0006-3495(04)74380-5
36. Seddon, J.M.: Structure of the inverted hexagonal (hii) phase, and non-lamellar phase transitions of lipids. Biochim. Biophys. Acta. Rev. Biomembr. **1031**(1), 1–69 (1990). doi:10.1016/0304-4157(90)90002-T
37. Turner, D., Gruner, S.: X-ray diffraction reconstruction of the inverted hexagonal (H_{ii}) phase in lipid–water systems. Biochemistry **31**, 1340–1355 (1992)
38. Hamm, M., Kozlov, M.: Tilt model of inverted amphiphilic mesophases. Eur. Phys. J. B Cond. Matter Complex Syst. **6**, 519–528 (1998). doi:10.1007/s100510050579
39. Templer, R.: Thermodynamic and theoretical aspects of cubic mesophases in nature and biological amphiphiles. Curr. Opin. Colloid Interface Sci. **3**, 255–263 (1998)

40. Kralj-Iglič, V., Babnik, B., Gauger, D., May, S., Iglič, A.: Quadrupolar ordering of phospholipid molecules in narrow necks of phospholipid vesicles. J. Stat. Phys. **125**, 727–752 (2006). doi: 10.1007/s10955-006-9051-9
41. Fournier, J.: Nontopological saddle-splay and curvature instabilities from anisotropic membrane inclusions. Phys. Rev. Lett. **76**, 4436–4439 (1996)
42. Helfrich, W.: Elastic properties of lipid bilayers—theory and possible experiments. Z. Nat. **28c**, 693–703 (1973)
43. Chen, Z., Rand, R.: The influence of cholesterol on phospholipid membrane curvature and bending elasticity. Biophys. J. **73**, 267–276 (1997)
44. Kirkpatrick, S., Gelatt, C., Vecchi, M.: Optimization by simulated annealing. Science **220**, 671–680 (1983)
45. Browicz, T.: Further observation of motion phenomena on red blood cells in pathological states. Zbl. Med. Wissen **28**(1), 625–627 (1890)
46. Menger, F.M., Keiper, J.S.: Chemistry and physics of giant vesicles as biomembrane models. Curr. Opin. Chem. Biol. **2**(6), 726–732 (1998). doi:10.1016/S1367-5931(98)80110-5
47. Noguchi, H.: Membrane simulation models from nanometer to micrometer scale. J. Phys. Soc. Jpn. **78**(4), 041,007 (2009)
48. Gompper, G., Kroll, D.M.: Random surface discretizations and the renormalization of the bending rigidity. J. Phys. I **6**(10), 1305–1320 (1996)
49. Gompper, G., Kroll, D.M.: Triangulated-surface models of fluctuating membranes. In: Nelson, D., Piran, T., Weinberg, S. (eds.) Statistical Mechanics of Membranes and Surfaces, 2nd edn. World Scientific, Singapore (2004)
50. Helfrich, W.: Elastic properties of lipid bilayers: theory and possible experiments. Z. Nat. **28**, 693–703 (1973)
51. Espriu, D.: Triangulated random surfaces. Phys. Lett. B **194**(2), 271–276 (1987)
52. Itzykson, C.: Random geometry, lattices and fields. In: Jabad, J., Asorey, M., Cruz, A. (eds.) Proceedings of the GIFT Seminar, Jaca 85, pp. 130–188. World scientific, Singapore (1986)
53. Milner, S.T., Safran, S.A.: Dynamical fluctuations of droplet microemulsions and vesicles. Phys. Rev. A **36**(9), 4371–4379 (1987). doi:10.1103/PhysRevA.36.4371
54. Bivas, I.: Elasticity and shape equation of a liquid membrane. Eur. Phys. J. B Cond. Matter Complex Syst. **29**(2), 317–322 (2002)